

Electronic Supplementary Material (ESI) for *Chem. Commun.*

This journal is © The Royal Society of Chemistry 2014

## Determination of the Magnetic Anisotropy in a Multinuclear Tb<sup>III</sup>-Based Single-Molecule Magnet

Xing-Cai Huang,<sup>[a]</sup> Veaceslav Vieru,<sup>[b]</sup> Liviu F Chibotaru,<sup>\*[b]</sup> Wolfgang Wernsdorfer,<sup>[c]</sup> Shang-Da Jiang,<sup>\*[d]</sup> and Xin-Yi Wang<sup>\*[a]</sup>

# Supporting Information

## Table of contents

<b>1. Experimental Section</b> .....	4
<b>1.1. Materials and methods</b> .....	4
<b>1.2. Preparation of [Cu<sub>2</sub>(<i>R</i>, <i>R</i>-valchxn)<sub>2</sub>Tb<sub>2</sub>(N<sub>3</sub>)<sub>6</sub>]•2CH<sub>3</sub>OH, <b>1-RR</b></b> .....	4
<b>1.3. Preparation of [Cu<sub>2</sub>(<i>S</i>, <i>S</i>-valchxn)<sub>2</sub>Tb<sub>2</sub>(N<sub>3</sub>)<sub>6</sub>]•2CH<sub>3</sub>OH, <b>1-SS</b></b> .....	4
<b>2. Solid-state Circular Dichroism (CD) spectra</b> .....	5
<b>Figure S1. Solid-state CD spectra of the compounds <b>1-RR</b> and <b>1-SS</b></b> .....	5
<b>3. X-ray crystallography</b> .....	5
<b>3.1. Single crystal X-ray data collection, structure solution and refinement for <b>1-RR</b> and <b>1-SS</b></b> .....	5
<b>Table S1. Crystallographic data for <b>1-RR</b> and <b>1-SS</b></b> .....	6
<b>Table S2. Selected Bond Lengths (Å) and Angles (°) for <b>1-RR</b> and <b>1-SS</b></b> .....	7
<b>3.2. Powder X-ray diffraction (PXRD) spectra</b> .....	9
<b>Figure S2. Experimental and calculated PXRD pattern of <b>1-RR</b></b> .....	9
<b>Figure S3. Experimental and calculated PXRD pattern of <b>1-SS</b></b> .....	9
<b>4. Magnetic Measurements</b> .....	10
<b>4.1. Measurements on the powder samples</b> .....	10
<b>Figure S4. Temperature dependent magnetic susceptibility of <b>1-RR</b> and <b>1-SS</b>. The solid line represents the theoretical simulation of the data (vide post). Experimental data were downscaled by 4%.</b> .....	10
<b>Figure S5. Field dependent magnetization curve of <b>1-RR</b> at 1.8 K. The solid line represents the calculated line (vide post)</b> .....	11
<b>Figure S6 Reduced magnetization of <b>1-RR</b></b> .....	11

<b>Figure S7.</b> Frequency dependence of the in-phase (top) and out-of-phase (bottom) ac susceptibilities for <b>1-RR</b> .....	12
<b>Table S3.</b> Relaxation fitting parameters from the least-square fitting of the Cole-Cole plots according to the generalized Debye model for <b>1-RR</b> .....	12
<b>Figure S8.</b> Hysteresis loops for a polycrystalline sample of <b>1-RR</b> with a sweep rate of 0.05 T/s at the indicated temperatures.....	13
<b>Figure S9.</b> Temperature dependence of the in-phase (top) and out-of-phase (bottom) ac susceptibilities for <b>1-SS</b> .....	13
<b>Figure S10.</b> Relaxation time of the magnetization $\ln(\tau)$ vs $T^{-1}$ plot of <b>1-SS</b> .....	14
<b>Figure S11.</b> Frequency dependence of the in-phase (top) and out-of-phase (bottom) ac susceptibilities for <b>1-SS</b> .....	14
<b>Figure S12.</b> Cole-Cole plots for <b>1-SS</b> from 3 to 16 K.....	15
<b>Table S4.</b> Relaxation fitting parameters from the least-square fitting of the Cole-Cole plots according to the generalized Debye model for <b>1-SS</b> .....	15
<b>4.2. Magnetic measurements on single crystals</b> .....	16
<b>4.2.1 Hysteresis loops on single crystals of 1-RR</b> .....	16
<b>Figure S13.</b> The hysteresis loops of <b>1-RR</b> measured on a field-oriented single crystal ( $m = 0.93$ mg) at the indicated temperatures and field sweep rates. ....	16
<b>Figure S14.</b> The derivative of the magnetization ( $d(M/M_s)/dH$ ) versus magnetic field for the curves measured at 0.03-4.0 K at a sweep rate of 0.14 T/s.....	17
<b>Figure S15.</b> The derivative of the magnetization ( $d(M/M_s)/dH$ ) versus magnetic field for the curves measured at 0.03 K at sweep rates of 0.001-0.28 T/s.....	17
<b>4.2.2 Angular dependent magnetic measurements of 1-RR</b> .....	18
<b>Figure S16.</b> The image of the single crystal of <b>1-RR</b> and the relationship of the abc and xyz reference frame.....	19
<b>Figure S17.</b> Angular dependence of magnetic susceptibility at $H = 1$ kOe for the rotations along the $x$ axes at different temperatures.....	19
<b>Figure S18.</b> Angular dependence of magnetic susceptibility at $H = 1$ kOe for the rotations along the $y$ axes at different temperatures.....	20
<b>Figure S19.</b> Angular dependence of magnetic susceptibility at $H = 1$ kOe for the rotations along the $z$ axes at different temperatures.....	20
<b>Figure S20.</b> Temperature dependent $\chi_M T$ curves along the easy, media and hard axes .....	21
<b>Table S5.</b> The magnetic susceptibility tensors, diagonalized tensors and eigenvectors in abc space at different temperatures.....	22
<b>5. Theoretical Calculations</b> .....	26
<b>5.1. Computational details</b> .....	26
<b>Figure S21.</b> Structure of compound <b>1-RR</b> for the ab initio calculation.....	26
<b>Table S6.</b> Contractions of the employed basis set.....	27
<b>5.2. Electronic and magnetic properties of individual Tb center in 1-RR</b> .....	27
<b>Table S7.</b> Energies of the low-lying spin-orbital states ( $\text{cm}^{-1}$ ) of Tb centers.....	27
<b>Table S8.</b> The $g_z$ values of the ground and first excited doublets of Tb centers....	28
<b>5.3. Account of magnetic interactions for compound 1-RR</b> .....	28

Table S9. Exchange and dipolar coupling parameters ( $\text{cm}^{-1}$ ) between magnetic ions in <b>1-RR</b> .....	28
Table S10. Energies ( $\text{cm}^{-1}$ ) of the low-lying exchange states of <b>1-RR</b> .....	29
<b>5.4. Details of electrostatic model calculation</b> .....	30
5.4.1. $\text{Tb}^{\text{III}}$ ion electron density.....	30
5.4.2. Electrostatic potential.....	30
5.4.3. Minimizing the potential energy.....	30
Figure S22. The bicapped trigonal prism of the $\text{Tb}^{3+}$ center and the calculated crystal field potential energy surface.....	31
<b>6. References</b> .....	31

# 1. Experimental Section

## 1.1. Materials and methods.

All preparations and manipulations were performed under aerobic conditions. The Schiff base ligands *R*, *R*-H<sub>2</sub>valchxn and *S*, *S*-H<sub>2</sub>valchxn were synthesized by the condensation of *N*, *N'*-(1*R*, 2*R*)-cyclohexanediamine or *N*, *N'*-(1*S*, 2*S*)-cyclohexanediamine with 3-methoxysalicylaldehyde. Compounds Cu(*R*, *R*-valchxn)·H<sub>2</sub>O and Cu(*S*, *S*-valchxn)·H<sub>2</sub>O were synthesized following the reported method.<sup>S1</sup> Elemental analyses were carried out on a Vario EL II Elementar. Infrared spectra were obtained on a Bruker Tensor 27 FT-IR spectrometer.

*Caution! Although our samples never exploded during handling, azido metal complexes are potentially explosive. Only a small amount of material should be prepared, and it should be handled with care.*

## 1.2. Preparation of [Cu<sub>2</sub>(*R*, *R*-valchxn)<sub>2</sub>Tb<sub>2</sub>(N<sub>3</sub>)<sub>6</sub>]·2CH<sub>3</sub>OH, 1-*RR*

A solution of Cu(*R*, *R*-valchxn)·H<sub>2</sub>O (46 mg, 0.1 mmol) and TbCl<sub>3</sub>·6H<sub>2</sub>O (38 mg, 0.1 mmol) in 5 mL of methanol was layered with a solution of NaN<sub>3</sub> (33 mg, 0.5 mmol) in 5 mL methanol. The resultant brown solution was left undisturbed. Dark black block-shaped crystals suitable for single crystal X-ray diffraction formed after one day. The crystals were filtered off, washed with methanol, and dried in air. Yield: 78 mg, 51%. Elemental analysis for [Cu<sub>2</sub>(valchxn)<sub>2</sub>Tb<sub>2</sub>(N<sub>3</sub>)<sub>6</sub>]·2CH<sub>3</sub>OH (C<sub>46</sub>H<sub>56</sub>N<sub>22</sub>O<sub>10</sub>Cu<sub>2</sub>Tb<sub>2</sub>): calcd. (found) C, 36.30 (36.14); N, 20.25 (20.14); H, 3.71 (3.80) %. IR (KBr pellets, cm<sup>-1</sup>): 2073(vs), 2056 (vs) for ν(N<sub>3</sub><sup>-</sup>).

## 1.3. Preparation of [Cu<sub>2</sub>(*S*, *S*-valchxn)<sub>2</sub>Tb<sub>2</sub>(N<sub>3</sub>)<sub>6</sub>]·2CH<sub>3</sub>OH, 1-*SS*

The same procedure was used to synthesize 1-*SS* except that Cu(*S*, *S*-valchxn)·H<sub>2</sub>O was used. Yield: 76 mg, 50 %. Elemental analysis for [Cu<sub>2</sub>(valchxn)<sub>2</sub>Tb<sub>2</sub>(N<sub>3</sub>)<sub>6</sub>]·2CH<sub>3</sub>OH (C<sub>46</sub>H<sub>56</sub>N<sub>22</sub>O<sub>10</sub>Cu<sub>2</sub>Tb<sub>2</sub>): calcd. (found) C, 36.30 (36.23); N, 20.25 (20.08); H, 3.71 (3.86)%. IR (KBr pellets, cm<sup>-1</sup>): 2073(vs), 2056 (vs) for ν(N<sub>3</sub><sup>-</sup>).

## 2. Solid-state Circular Dichroism (CD) spectra

Solid state CD spectra were recorded with a JASCO J-810 spectropolarimeter. For the solid state CD spectra, crystalline samples were ground to fine powders with potassium chloride and compressed into transparent disks and the concentration of the complexes was 1.0 mg/400 mg KCl.<sup>S2</sup>

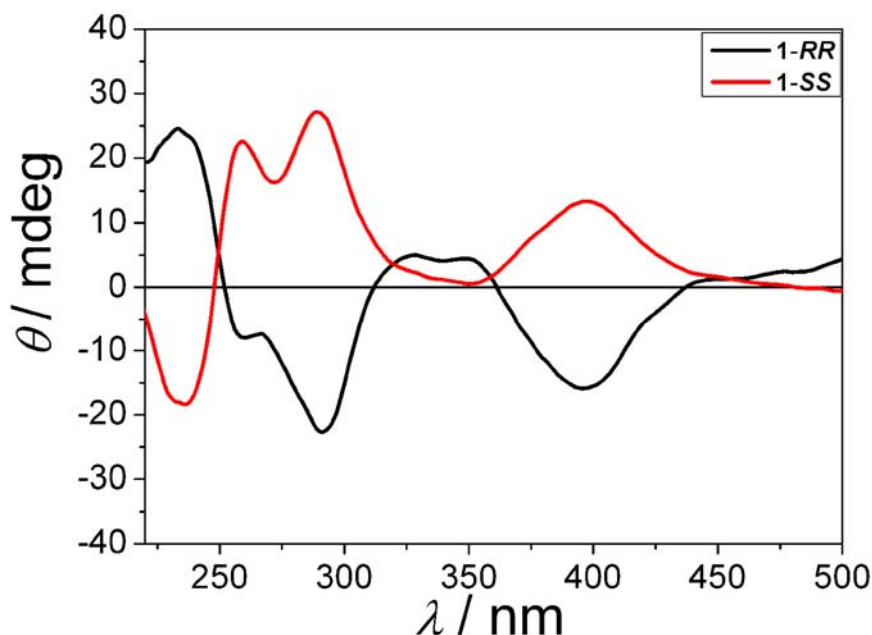


**Figure S1.** Solid-state CD spectra of the compounds **1-RR** and **1-SS**.

## 3. X-ray crystallography

### 3.1. Single crystal X-ray data collection, structure solution and refinement for **1-RR** and **1-SS**

The single crystal X-ray data of **1-RR** and **1-SS** were collected on a Bruker APEX DUO diffractometer with a CCD area detector (Mo-K $\alpha$  radiation,  $\lambda = 0.71073$  Å). The APEX II program was used to determine the unit cell parameters and for data collection. The data were integrated using SAINT<sup>S3</sup> and SADABS.<sup>S4</sup> The structures for both compounds were solved by direct methods and refined by full-matrix least-squares based on  $F^2$  using the SHELXTL program.<sup>S5</sup> All the non-hydrogen atoms were refined anisotropically. Hydrogen atoms of the organic ligands were refined as riding on the corresponding non-hydrogen atoms. Hydrogen atoms of the

OH groups of the methanol are located from the difference Fourier maps and refined isotropically. Additional details of the data collections and structural refinement parameters are provided in Table S1. Selected bond lengths and bond angles are listed in Table S2. CCDC 1000153–1000154 contain the supplementary crystallographic data for this paper. These data can be obtained free of charge from The Cambridge Crystallographic Data Centre via [www.ccdc.cam.ac.uk/data\\_request/cif](http://www.ccdc.cam.ac.uk/data_request/cif) and the Supporting Information of this paper.

**NOTE:** Since we used the enantiopure starting materials for the synthesis, the resulting compounds are chiral as confirmed by their CD spectra in Figure S1. Thus, the crystals of **1-RR** and **1-SS** were solved in a chiral space group *P1*. This leads to the “Alert A” and “Alert B” warnings in the CheckCIF file. The triclinic space group *P1* is also the reason for the poor Data / Parameter Ratio.

**Table S1.** Crystallographic data for **1-RR** and **1-SS**

Complex	<b>1-RR</b>	<b>1-SS</b>
Formula	Cu <sub>2</sub> Tb <sub>2</sub> C <sub>46</sub> H <sub>56</sub> N <sub>22</sub> O <sub>10</sub>	Cu <sub>2</sub> Tb <sub>2</sub> C <sub>46</sub> H <sub>56</sub> N <sub>22</sub> O <sub>10</sub>
CCDC number	1000153	1000154
Mr [g mol <sup>-1</sup> ]	1522.05	1522.05
Crystal size [mm <sup>3</sup> ]	0.39×0.25×0.06	0.72×0.39×0.09
Crystal system	Triclinic	Triclinic
Space group	<i>P1</i>	<i>P1</i>
<i>a</i> [Å]	9.64950(10)	9.6455(2)
<i>b</i> [Å]	11.9679(2)	11.9723(3)
<i>c</i> [Å]	12.5126(2)	12.5139(3)
<i>α</i> [°]	78.8790(10)	78.8640(10)
<i>β</i> [°]	85.4400(10)	85.3970(10)
<i>γ</i> [°]	79.3090(10)	79.2560(10)
<i>V</i> [Å <sup>3</sup> ]	1391.83(4)	1391.56(6)
<i>Z</i>	1	1
<i>T</i> , K	293(2)	293(2)
$\rho_{\text{calcd}}$ [g cm <sup>-3</sup> ]	1.806	1.816
$\mu$ (Mo–K $\alpha$ ) [mm <sup>-1</sup> ]	3.339	3.340
<i>F</i> (000)	746	754
$\theta$ range [°]	1.66–25.00	1.66–27.49
Refl. collected / unique	19222 / 9109	22445 / 9850
<i>R</i> (int)	0.0216	0.0296
<i>T</i> <sub>max</sub> / <i>T</i> <sub>min</sub>	0.8248 / 0.3559	0.7531 / 0.1704
Data/restraints/ parameters	9109 / 334 / 754	9850 / 334 / 753

$R_1^a/wR_2^b$ ( $I > 2\sigma(I)$ )	0.0242 / 0.0641	0.0290 / 0.0773
$R_1/wR_2$ (all data)	0.0261 / 0.0659	0.0313 / 0.0793
GOF on $F^2$	1.014	1.055
Max/min [ $e \text{ \AA}^{-3}$ ]	0.537 / -0.563	0.856 / -0.550

$$^a R_1 = \sum ||F_o| - |F_c|| / \sum |F_o|, ^b wR_2 = \{ \sum [w(F_o^2 - F_c^2)^2] / \sum [w(F_o^2)^2] \}^{1/2}$$

**Table S2.** Selected Bond Lengths (Å) and Angles (°) for **1-RR** and **1-SS**

<b>1-RR</b>					
<b>Selected Bond Lengths (Å)</b>					
Tb1-O1	2.343(6)	Tb1-O3	2.590(6)	Tb2-N20	2.392(9)
Tb1-O2	2.354(6)	Tb1-O4	2.592(6)	Tb2-N5	2.502(7)
Tb1-N11	2.349(8)	Tb2-O6	2.316(6)	Tb2-O8	2.559(6)
Tb1-N14	2.379(9)	Tb2-O5	2.346(7)	Tb2-O7	2.631(6)
Tb1-N5	2.426(7)	Tb2-N8	2.427(7)	Cu1-N2	1.916(9)
Tb1-N8	2.442(8)	Tb2-N17	2.379(8)	Cu2-N3	1.916(8)
Cu1-O1	1.911(7)	Cu1-O2	1.901(7)	Cu2-O6	1.914(6)
Cu1-N1	1.925(7)	Cu2-O5	1.923(6)	Cu2-N4	1.944(7)
Tb1...Cu1	3.3989(14)	Tb2...Cu2	3.4047(13)		
<b>Selected Bond Angles (°)</b>					
O1-Tb1-O2	65.0(2)	N11-Tb1-N14	87.7(3)	O2-Tb1-N5	81.9(2)
O1-Tb1-N11	147.8(3)	O2-Tb1-N14	85.1(3)	N14-Tb1-N5	147.3(3)
O2-Tb1-N11	146.3(3)	O1-Tb1-N5	112.3(2)	O1-Tb1-N8	82.7(3)
O1-Tb1-N14	88.6(3)	N11-Tb1-N5	86.8(3)	N11-Tb1-N8	82.0(3)
O2-Tb1-N8	120.9(3)	N11-Tb1-O3	86.4(3)	N8-Tb1-O3	72.1(2)
N14-Tb1-N8	144.6(3)	O2-Tb1-O3	122.5(2)	O1-Tb1-O4	124.5(2)
N5-Tb1-N8	66.0(2)	N14-Tb1-O3	73.5(3)	N11-Tb1-O4	84.7(3)
O1-Tb1-O3	61.9(2)	N5-Tb1-O3	138.1(2)	O2-Tb1-O4	61.8(2)
N14-Tb1-O4	72.8(3)	N5-Tb1-O4	74.6(2)	N8-Tb1-O4	138.9(2)
O3-Tb1-O4	145.4(2)	N20-Tb2-O7	73.5(3)	N8-Tb2-O7	74.0(2)
O6-Tb2-O5	65.2(2)	O5-Tb2-N20	83.8(3)	N17-Tb2-N8	87.0(3)
O6-Tb2-N17	148.0(3)	N17-Tb2-N20	87.2(3)	N20-Tb2-N8	147.4(3)
O5-Tb2-N17	145.9(3)	O6-Tb2-N8	110.6(3)	O6-Tb2-N5	82.6(2)
O6-Tb2-N20	90.6(3)	O5-Tb2-N8	83.2(3)	O5-Tb2-N5	122.9(2)
N17-Tb2-N5	81.1(3)	O5-Tb2-O8	122.5(2)	N5-Tb2-O8	72.8(2)
N20-Tb2-N5	145.0(3)	N17-Tb2-O8	85.8(3)	O6-Tb2-O7	125.1(2)
N8-Tb2-N5	65.1(2)	N20-Tb2-O8	73.6(3)	O5-Tb2-O7	61.1(2)
O6-Tb2-O8	63.0(2)	N8-Tb2-O8	137.8(2)	N17-Tb2-O7	84.8(3)
N5-Tb2-O7	137.2(2)	O8-Tb2-O7	146.0(2)		
O2-Cu1-O1	82.8(3)	O1-Cu1-N1	94.0(3)	O6-Cu2-N3	170.2(3)

O2-Cu1-N2	94.7(3)	N2-Cu1-N1	88.1(3)	O6-Cu2-O5	81.7(3)
O1-Cu1-N2	176.8(3)	O6-Cu2-N4	96.7(3)	N3-Cu2-O5	95.9(3)
O2-Cu1-N1	171.6(3)	O5-Cu2-N4	176.3(3)	N3-Cu2-N4	85.2(3)

### 1-SS

Selected Bond Lengths (Å)					
Tb1-O1	2.327(8)	Tb1-N5	2.446(8)	Tb2-O6	2.344(9)
Tb1-O2	2.346(8)	Tb1-N8	2.441(10)	Tb2-O5	2.363(8)
Tb1-N11	2.342(10)	Tb1-O3	2.599(8)	Tb2-N17	2.392(11)
Tb1-N14	2.409(12)	Tb1-O4	2.610(8)	Tb2-N20	2.369(12)
Tb2-N8	2.417(10)	Cu1-O1	1.896(9)	Cu2-N3	1.901(11)
Tb2-N5	2.509(8)	Cu1-O2	1.907(9)	Cu2-N4	1.936(10)
Tb2-O8	2.555(9)	Cu1-N1	1.923(11)	Cu2-O5	1.911(8)
Tb2-O7	2.625(9)	Cu1-N2	1.934(10)	Cu2-O6	1.925(8)
Tb1...Cu1	3.3995(16)	Tb2...Cu2	3.4132(16)		

Selected Bond Angles (°)					
O1-Tb1-O2	64.5(3)	N11-Tb1-N14	88.4(4)	O2-Tb1-N8	120.7(3)
O1-Tb1-N11	148.0(4)	O2-Tb1-N14	84.7(4)	N14-Tb1-N8	145.4(4)
N11-Tb1-O2	146.6(3)	O1-Tb1-N8	83.2(4)	O1-Tb1-N5	112.0(3)
O1-Tb1-N14	88.4(4)	N11-Tb1-N8	81.6(4)	N11-Tb1-N5	86.8(4)
O2-Tb1-N5	81.7(3)	N11-Tb1-O3	86.3(4)	N5-Tb1-O3	138.0(3)
N14-Tb1-N5	147.0(4)	O2-Tb1-O3	122.6(3)	O1-Tb1-O4	123.7(3)
N8-Tb1-N5	65.6(3)	N14-Tb1-O3	74.0(4)	N11-Tb1-O4	85.5(4)
O1-Tb1-O3	62.3(3)	N8-Tb1-O3	72.4(3)	O2-Tb1-O4	61.3(3)
N14-Tb1-O4	72.8(4)	N8-Tb1-O4	138.3(3)	N5-Tb1-O4	74.3(3)
O3-Tb1-O4	146.0(3)	N17-Tb2-O7	84.4(4)	N8-Tb2-O7	74.5(3)
O6-Tb2-O5	65.2(3)	O5-Tb2-N17	146.0(3)	N20-Tb2-N8	148.0(4)
O6-Tb2-N20	90.8(4)	N20-Tb2-N17	86.6(4)	N17-Tb2-N8	86.9(4)
O5-Tb2-N20	84.4(4)	O6-Tb2-N8	110.6(3)	O6-Tb2-N5	82.1(3)
O6-Tb2-N17	147.8(4)	O5-Tb2-N8	83.6(3)	O5-Tb2-N5	122.7(3)
N20-Tb2-N5	144.2(3)	O5-Tb2-O8	121.8(3)	N5-Tb2-O8	72.6(3)
N17-Tb2-N5	81.5(4)	N20-Tb2-O8	73.1(4)	O6-Tb2-O7	125.5(3)
N8-Tb2-N5	65.0(3)	N17-Tb2-O8	86.3(4)	O5-Tb2-O7	61.6(3)
O6-Tb2-O8	62.4(3)	N8-Tb2-O8	137.6(3)	N20-Tb2-O7	73.6(4)
N5-Tb2-O7	137.6(3)	O8-Tb2-O7	145.8(3)		
O1-Cu1-N2	176.2(4)	O2-Cu1-N2	95.0(4)	O1-Cu1-N1	94.5(4)
O1-Cu1-O2	82.0(3)	N1-Cu1-N2	88.3(4)	O2-Cu1-N1	172.3(4)
O5-Cu2-N4	176.1(4)	N3-Cu2-N4	85.0(4)	N3-Cu2-O5	95.6(4)
O5-Cu2-O6	82.7(3)	O6-Cu2-N4	96.1(4)	N3-Cu2-O6	170.3(4)

### 3.2. Powder X-ray diffraction (PXRD) spectra

Powder X-ray diffractions (PXRD) were recorded at 298 K on a Bruker D8 Advance diffractometer with Cu-K $\alpha$  X-ray source (operated at 40kV and 40mA).

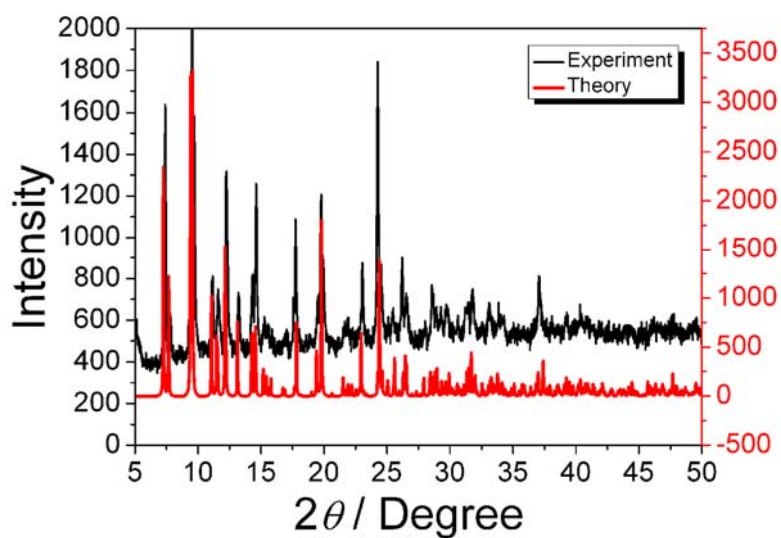


**Figure S2.** Experimental and calculated X-ray powder diffraction pattern of **1-RR**.

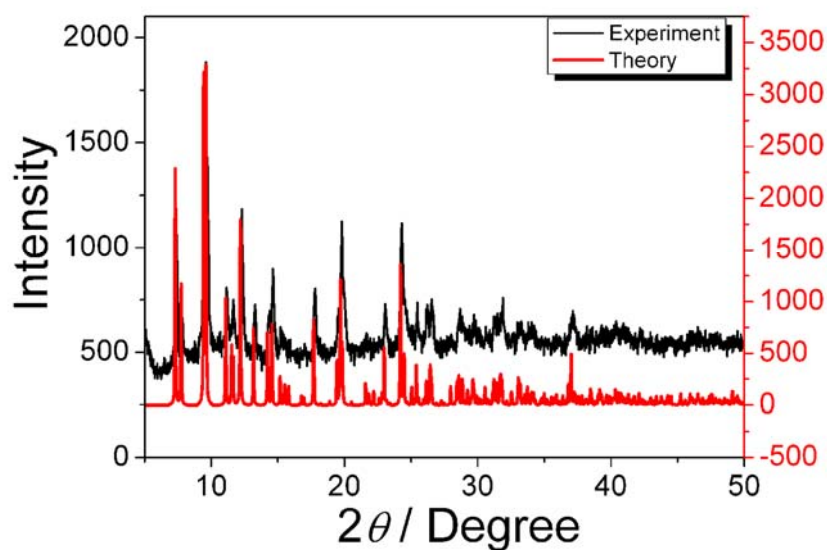


**Figure S3.** Experimental and calculated X-ray powder diffraction pattern of **1-SS**.

## 4. Magnetic Measurements.

### 4.1. Measurements on the powder samples.

Magnetic measurements were performed on powder samples for the two compounds embedded in eicosane with Quantum Design MPMS XL-7 or SQUID VSM magnetometers at temperatures ranging from 1.8 to 300 K with field up to 7 T. All data were corrected for diamagnetism of the eicosane, the sample holder, and the constituent atoms using Pascal's constants. The temperature and frequency dependent ac magnetic susceptibility data for **1-RR** and **1-SS** were collected using a 5 Oe ac field and a zero dc field.

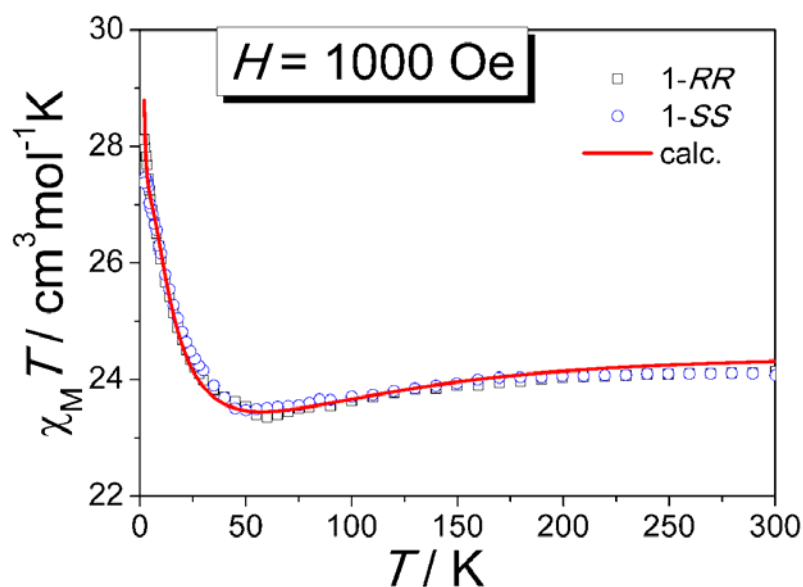


**Figure S4.** Temperature dependent magnetic susceptibility of **1-RR** and **1-SS**. The solid line represents the theoretical simulation of the data (vide post). Experimental data were downscaled by 4%.

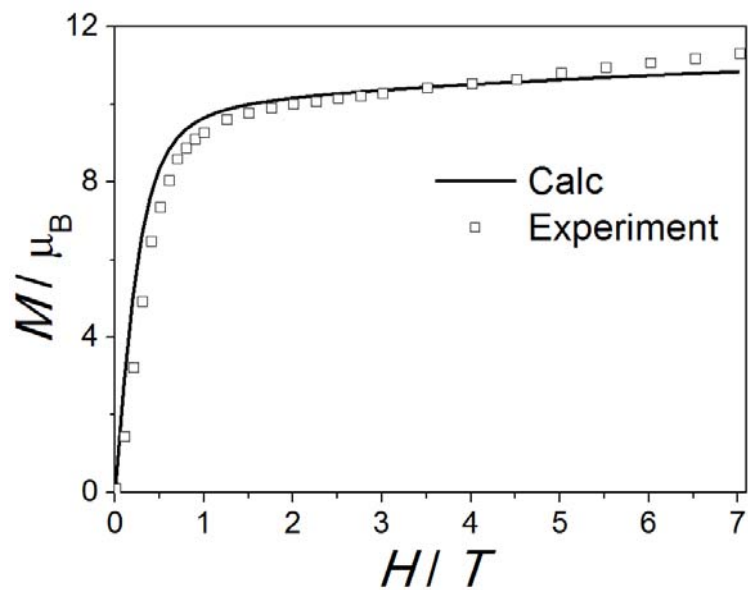


**Figure S5.** Field dependent magnetization curve of **1-RR** at 1.8 K. The solid line represents the calculated line (vide post).

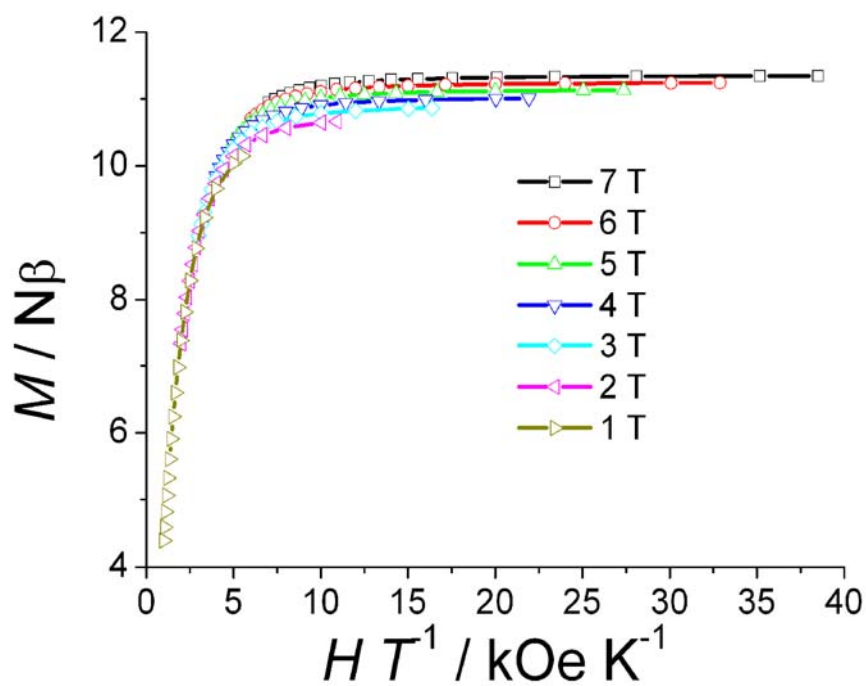


**Figure S6.** Reduced magnetization of **1-RR**.

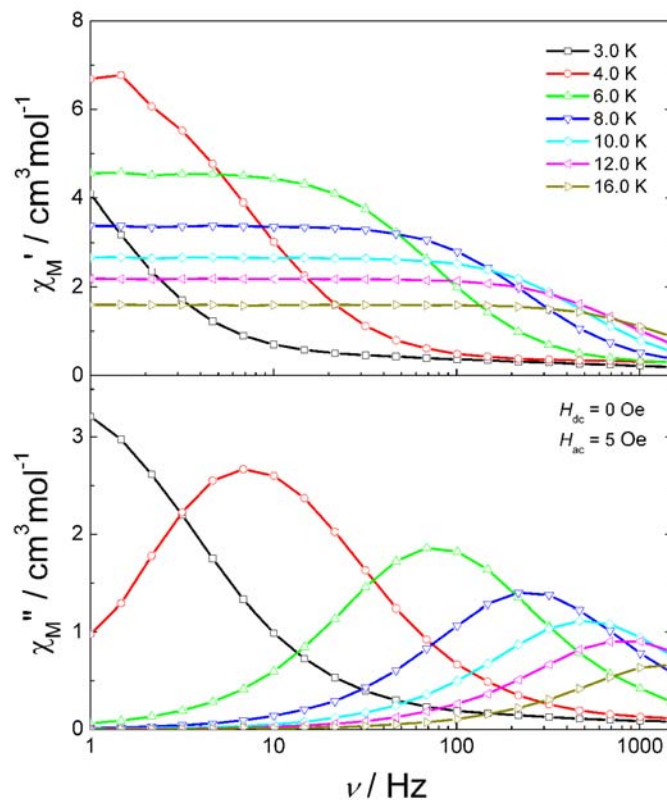


**Figure S7.** Frequency dependence of the in-phase (top) and out-of-phase (bottom) ac susceptibilities for **1-RR** ( $H_{dc} = 0\text{Oe}$ ,  $H_{ac} = 5\text{Oe}$ ).

**Table S3.** Relaxation fitting parameters from the least-square fitting of the Cole-Cole plots according to the generalized Debye model for **1-RR**

Temperature / K	$\chi_S / \text{cm}^3 \text{mol}^{-1} \text{K}$	$\chi_T / \text{cm}^3 \text{mol}^{-1} \text{K}$	$\tau / \text{s}$	$\alpha$
3.0	0.26219	8.81426	0.19386	0.17151
4.0	0.26726	6.99321	0.02143	0.13475
6.0	0.23398	4.57529	0.00204	0.08795
8.0	0.19171	3.38397	0.00064	0.07492
10.0	0.17192	2.66997	0.00031	0.06607
12.0	0.20894	2.18099	0.00020	0.04854
16.0	0.18158	1.59988	0.00011	0.03772

$\chi_S$ : adiabatic susceptibility;  $\chi_T$ : isothermal susceptibility;  $\tau$ : relaxation time;  $\alpha$ : variable representing the distribution of relaxation times.

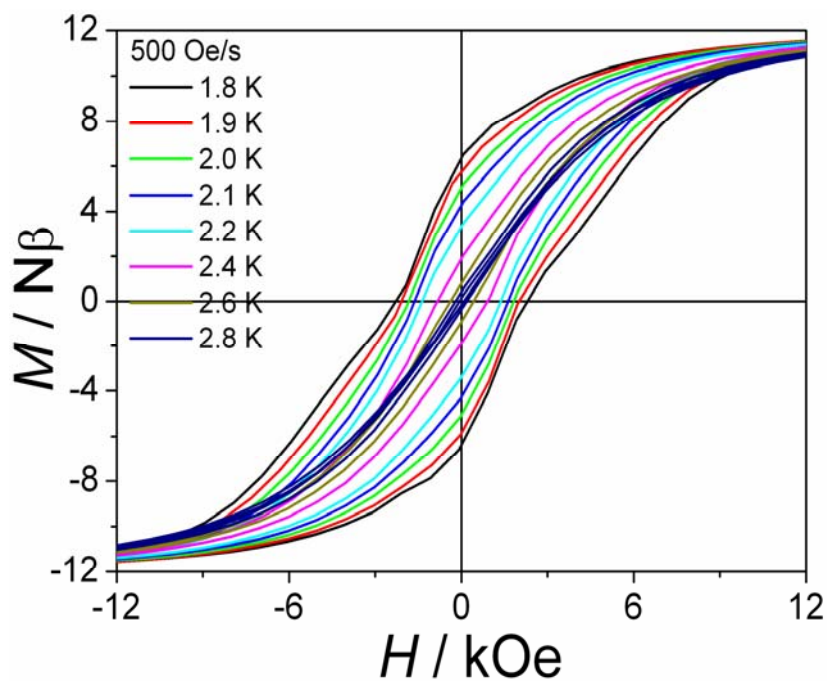


**Figure S8.** Hysteresis loops for a polycrystalline sample of **1-RR** with a sweep rate of 0.05 T/s at the indicated temperatures.

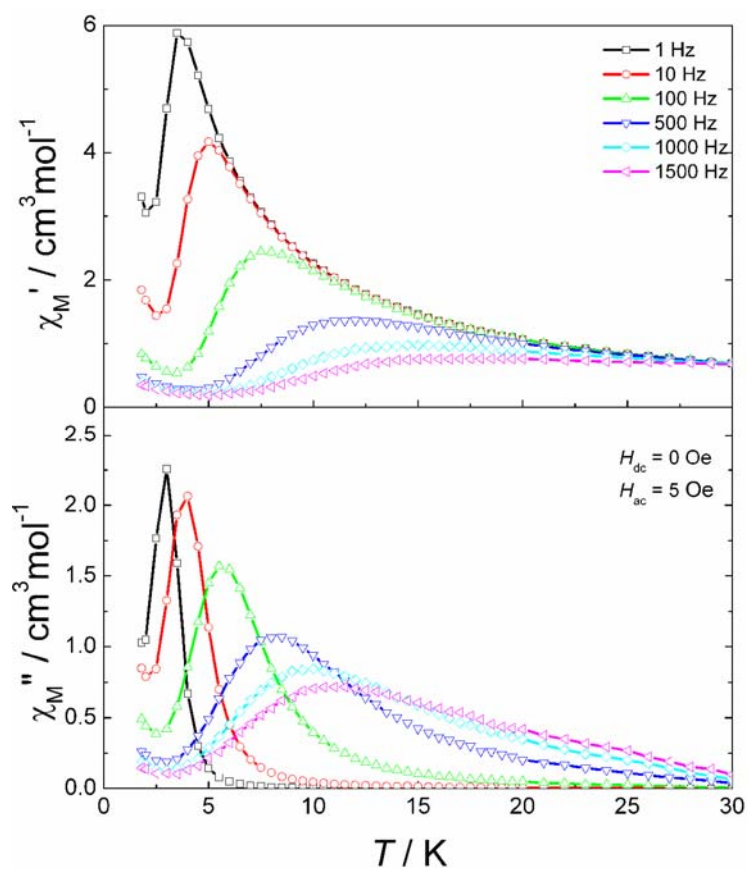


**Figure S9.** Temperature dependence of the in-phase (top) and out-of-phase (bottom) *a.c.* susceptibilities for **1-SS**.

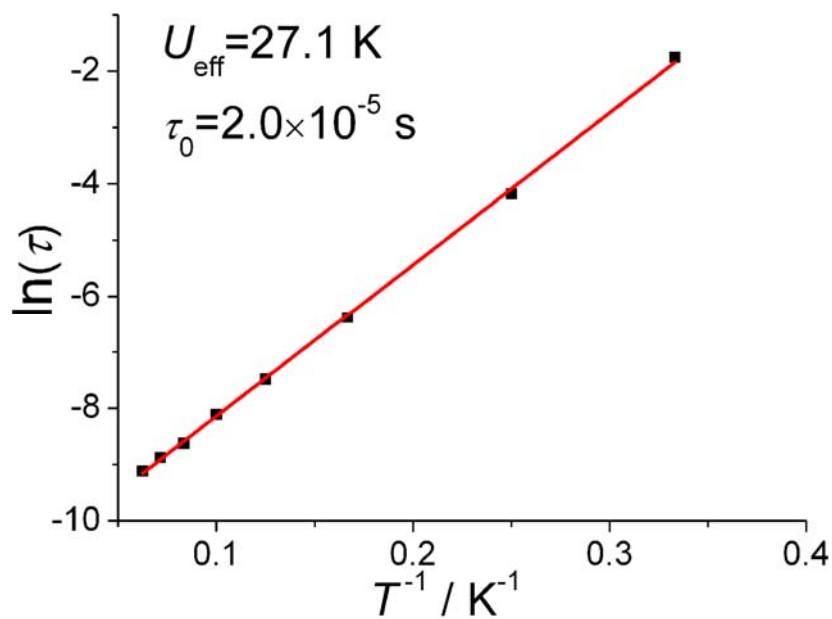


**Figure S10.** Relaxation time of the magnetization  $\ln(\tau)$  vs  $T^{-1}$  plot of **1-SS**; the red solid line corresponds to the Arrhenius law.

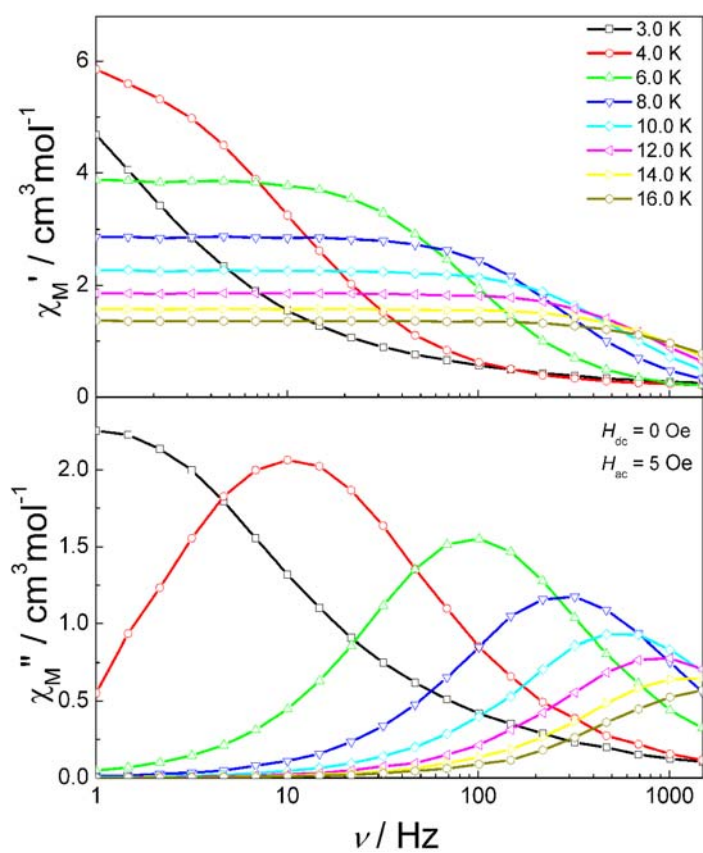


**Figure S11.** Frequency dependence of the in-phase (top) and out-of-phase (bottom) ac susceptibilities for **1-SS** ( $H_{\text{dc}} = 0 \text{ Oe}$ ,  $H_{\text{ac}} = 5 \text{ Oe}$ ).

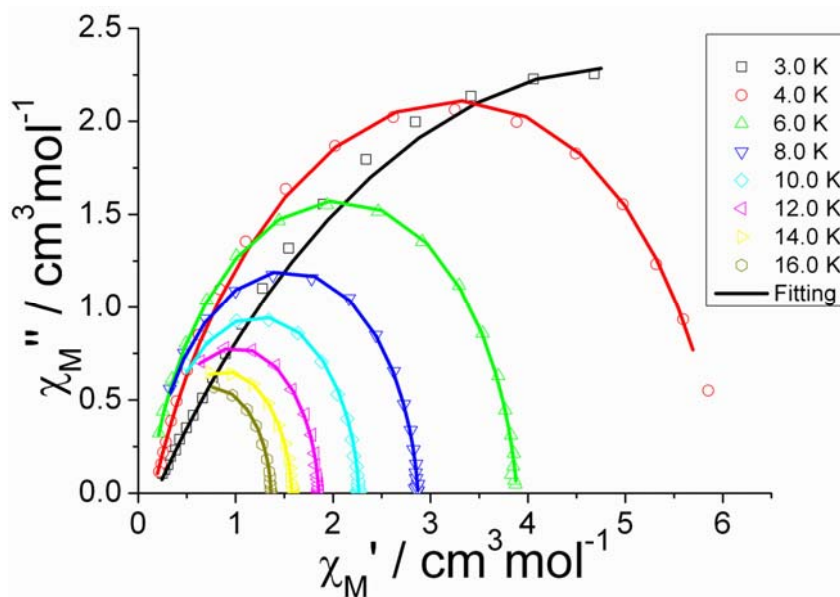


**Figure S12.** Cole-Cole plots for **1-SS** from 3 to 16 K ( $H_{dc} = 0$  Oe,  $H_{ac} = 5$  Oe). The lines represent the best fitting according to the generalized Debye model.

**Table S4.** Relaxation fitting parameters from the least-square fitting of the Cole-Cole plots according to the generalized Debye model for **1-SS**

Temperature / K	$\chi_S / \text{cm}^3 \text{mol}^{-1} \text{K}$	$\chi_T / \text{cm}^3 \text{mol}^{-1} \text{K}$	$\tau / \text{s}$	$\alpha$
3.0	0.18196	8.83738	0.17267	0.38108
4.0	0.15106	6.00709	0.01533	0.2045
6.0	0.1125	3.88678	0.00169	0.11476
8.0	0.11834	2.87109	$5.6 \times 10^{-4}$	0.08959
10.0	0.17739	2.26462	$3.0 \times 10^{-4}$	0.0604
12.0	0.13357	1.85295	$1.8 \times 10^{-4}$	0.06083
14.0	0.15714	1.57577	$1.4 \times 10^{-4}$	0.05151
16.0	0.13445	1.36257	$1.1 \times 10^{-4}$	0.04807

$\chi_S$ : adiabatic susceptibility;  $\chi_T$ : isothermal susceptibility;  $\tau$ : relaxation time;  $\alpha$ : variable representing the distribution of relaxation times.

## 4.2. Magnetic measurements on single crystals.

### 4.2.1. Hysteresis loops on single crystals of 1-RR.

SQUID-VSM measurement: One single crystal of **1-RR** ( $m = 0.93$  mg) was embedded in the eicosane. It was heated to 320 K (47 °C), and a strong magnetic field of 5 T was applied to align the crystal along its easy axis. The sample stayed at 320 K for 5 minutes and was cooled down to low temperature with the field on. Magnetic measurements were then performed on the aligned single crystal.

Magnetic hysteresis loops on one single crystal were also measured with a micro-SQUID from 4 to 0.03 K, with the field sweep rate from 0.001 to 0.280 T/s.

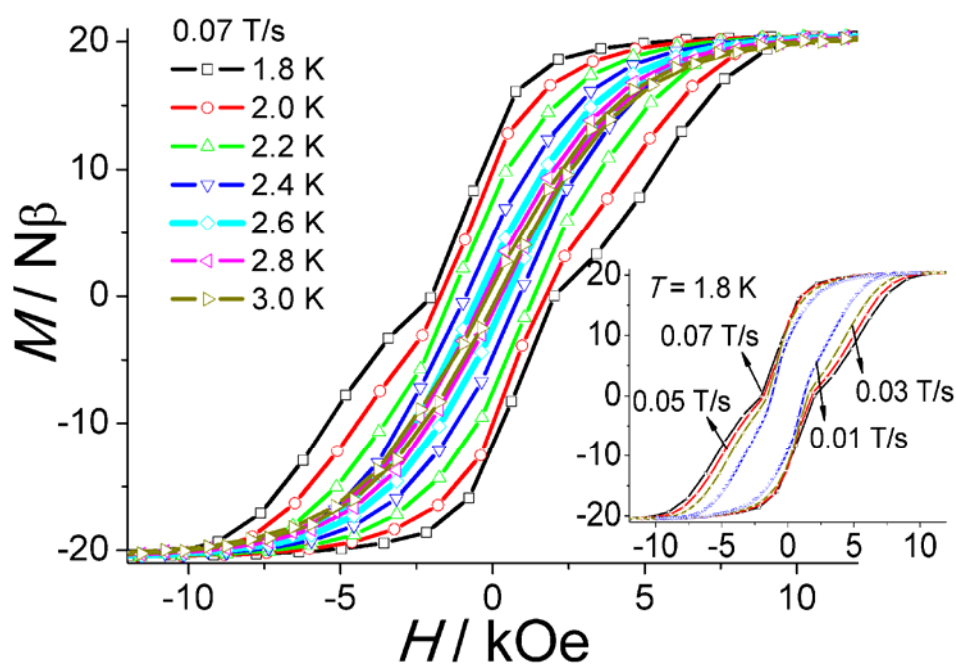


**Figure S13.** The hysteresis loops of **1-RR** measured on a field-oriented single crystal ( $m = 0.93$  mg) at the indicated temperatures and field sweep rates.

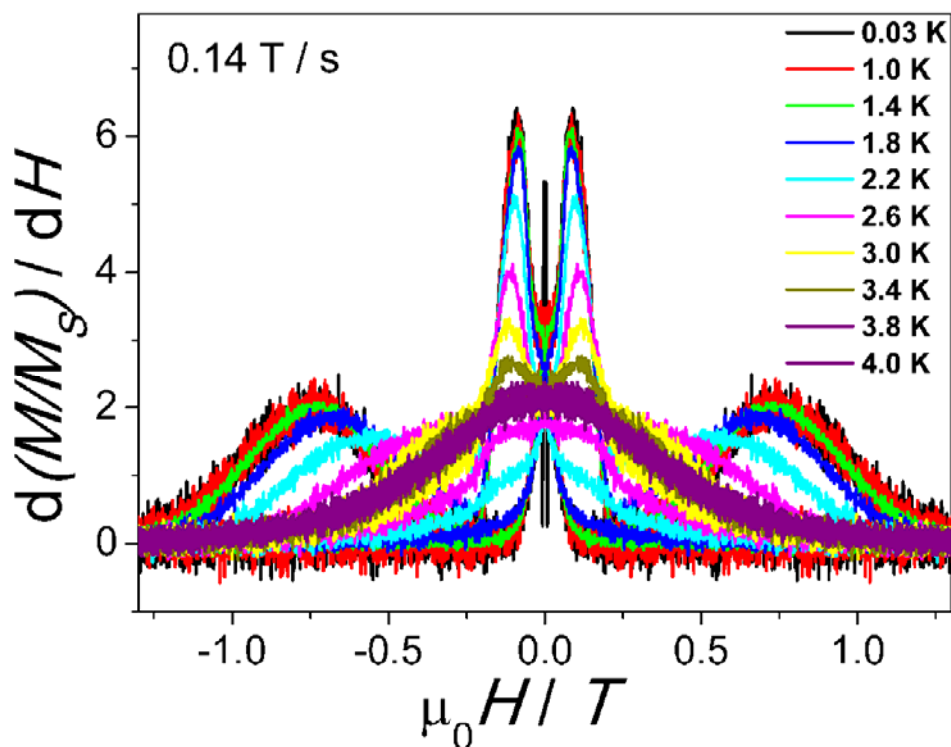


**Figure S14.** The derivative of the magnetization ( $d(M/M_s)/dH$ ) versus magnetic field for the curves measured at 0.03 - 4.0 K at a sweep rate of 0.14 T/s

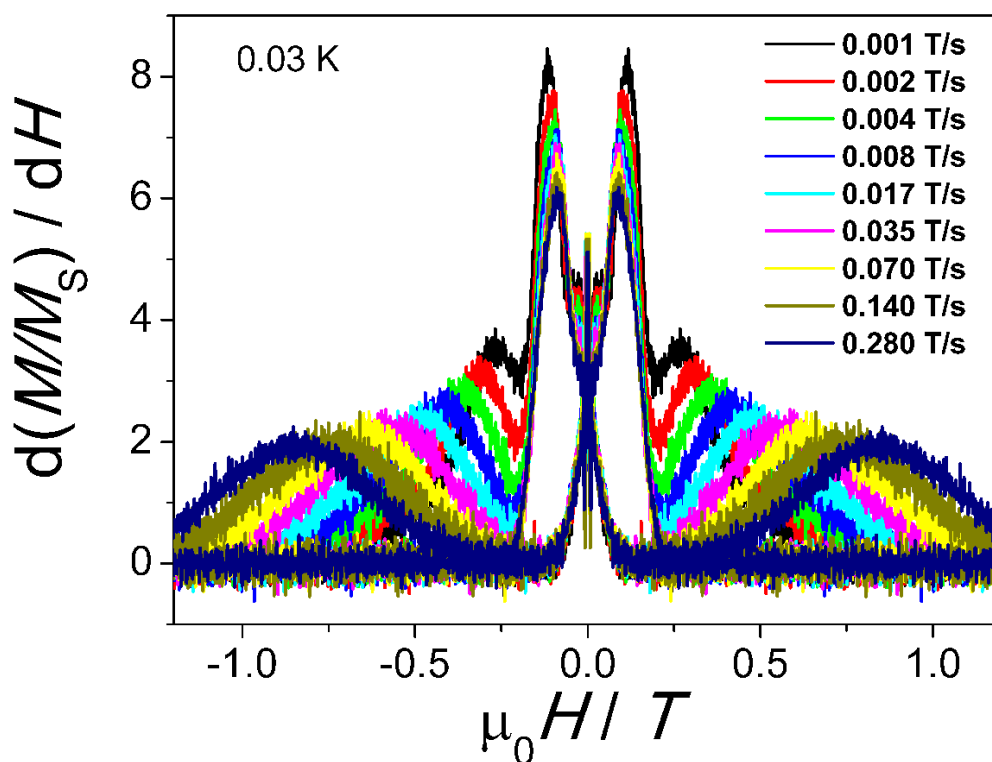


**Figure S15.** The derivative of the magnetization ( $d(M/M_s)/dH$ ) versus magnetic field for the curves measured at 0.03 K at sweep rates of 0.001 - 0.28 T/s

**4.2.2. Angular dependent magnetic measurements of 1-RR.** Angular-dependent magnetic measurements were performed on a horizontal rotator from Quantum Design, using the Quantum Design MPMS XL-7 SQUID magnetometer. A single crystal ( $m = 0.43$  mg) of **1-RR** was first face-indexed in a Bruker APEX II diffractometer (Figure S18). Then this crystal was glued, over its (100) face, onto an L-shaped Cu:Be support. The three orthogonal directions of the laboratory reference frame  $x$ ,  $y$ ,  $z$  are defined as follows:  $b$  direction is defined as  $x$  axis, which is the intersection of (001) and (-102); the (001) face is defined as  $xy$  plane; and  $z$  is defined by the right-hand rule (Figure S18). The transformation matrix between the laboratory reference frame ( $x, y, z$ ) and the crystal frame ( $a, b, c$ ) is as following:

$$\begin{pmatrix} a \\ b \\ c \end{pmatrix} = \begin{pmatrix} 1.78 & 9.41 & 0 \\ 11.93 & 0 & 0 \\ 2.40 & 0.71 & 12.18 \end{pmatrix} \begin{pmatrix} x \\ y \\ z \end{pmatrix}$$

Three orthogonal rotations along  $x$ ,  $y$ , and  $z$  directions were then performed at  $H_{dc} = 1$  kOe in the temperature range of 1.8 to 15 K (Figure S19 - S21). The diamagnetic background of the sample rotator and the beryllium copper slice was corrected from the signal of the magnetization.

The values of the components of the magnetic susceptibility were extracted by fitting the magnetization data from the rotation around three independent axes. Then, the susceptibility tensors in the reference frame ( $x, y, z$ ) were diagonalized to give the three principle components of the susceptibilities. The eigenvector matrix in the ( $x, y, z$ ) reference frame, which is according to the direction of the principle components were then transformed back to the ( $a, b, c$ ) system. The results were listed in Table S5.



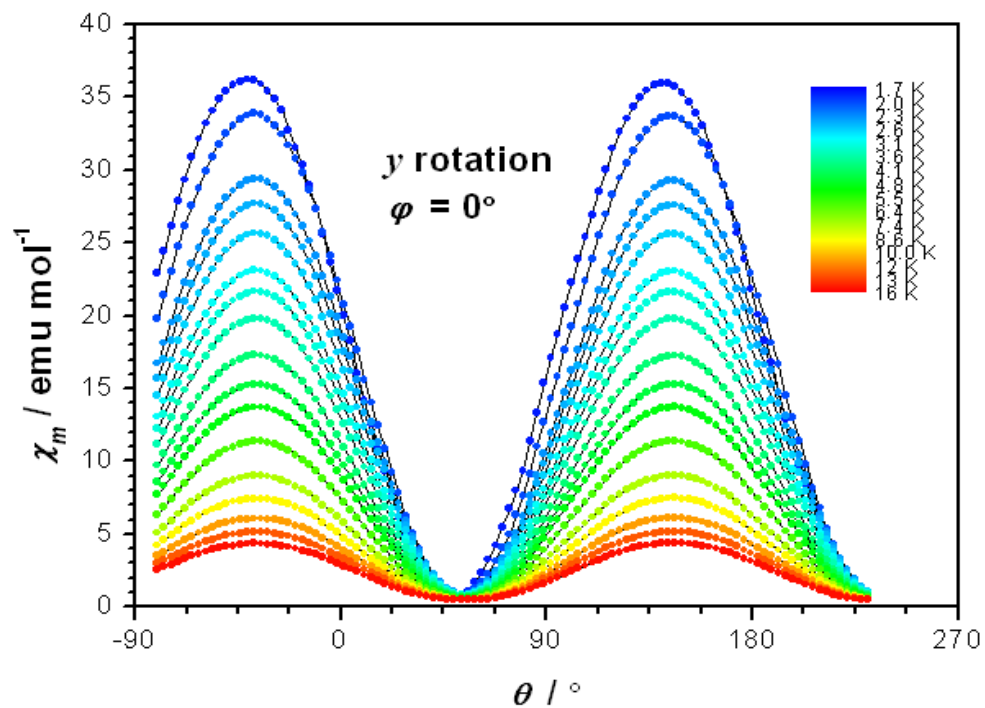


**Figure S18.** Rotation along the  $y$  axes (left) and angular dependence of magnetic susceptibility at  $H = 1$  kOe for the rotations along the  $y$  axes at different temperatures.

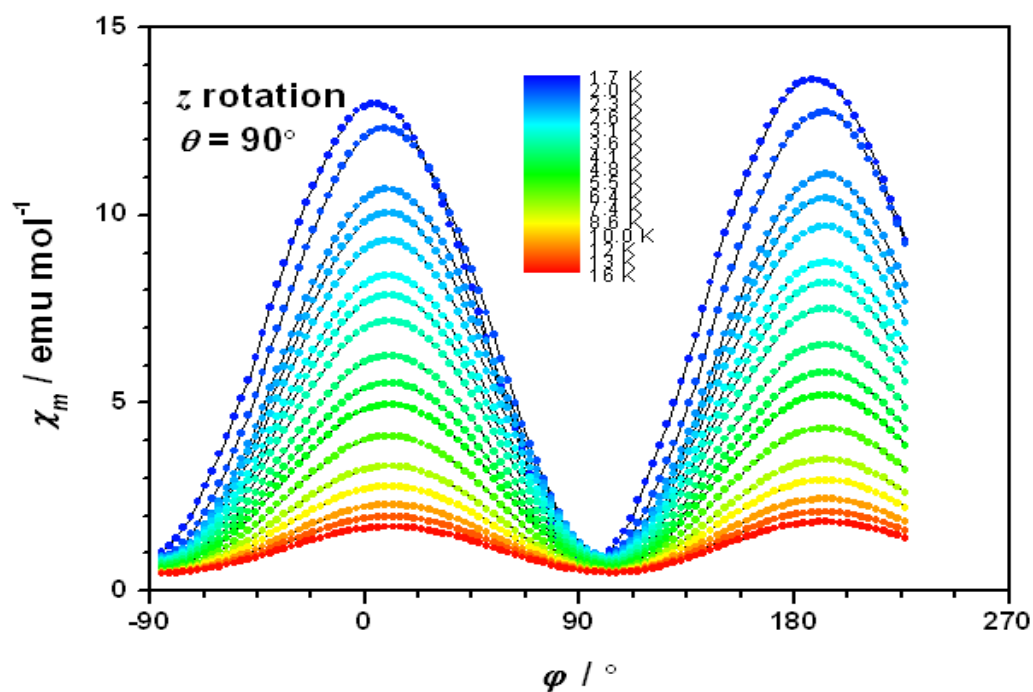
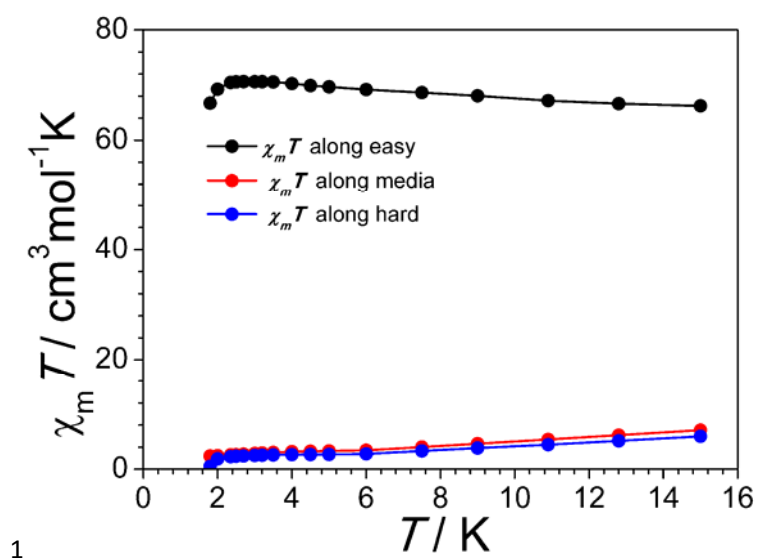


**Figure S19.** Rotation along the  $z$  axes (left) and angular dependence of magnetic susceptibility at  $H = 1$  kOe for the rotations along the  $z$  axes at different temperatures.



1

**Figure S20.** Temperature dependent  $\chi_M T$  curves along the easy, media and hard axes, showing the strong Ising anisotropy.

**Table S5.** The magnetic susceptibility tensors, diagonalized tensors and eigenvectors in *abc* space at different temperatures

<i>T</i> / K	Full tensors	Diagonalized tensors	Eigenvectors in <i>abc</i> space	
1.8	$\begin{pmatrix} 13.5101 & -3.43516 & -17.7478 \\ -3.43561 & 2.14573 & 5.1578 \\ -17.7478 & 5.1578 & 22.978 \end{pmatrix}$	$\begin{pmatrix} 37.6882 & & \\ & 1.19813 & \\ & & -0.252394 \end{pmatrix}$	Easy	{-0.0164857, -0.0593218, 0.0664437}
			Medium	{-0.102119, 0.00984252, -0.0168336}
			Hard	{0.0249881, -0.0625164, -0.0452197}
2.0	$\begin{pmatrix} 12.3777 & -2.56391 & -15.8904 \\ -2.56391 & 1.70348 & 3.41654 \\ -15.8904 & 3.41654 & 22.6919 \end{pmatrix}$	$\begin{pmatrix} 34.7925 & & \\ & 1.16466 & \\ & & 0.81601 \end{pmatrix}$	Easy	{-0.00865461, 0.0634406, -0.0658661}
			Medium	{-0.104772, 0.0187657, 0.0174893}
			Hard	{0.0165033, 0.0561016, 0.0458119}
2.35	$\begin{pmatrix} 10.6567 & -2.04872 & -13.5883 \\ -2.04872 & 1.47393 & 2.5945 \\ -13.5883 & 2.5945 & 19.9202 \end{pmatrix}$	$\begin{pmatrix} 30.0264 & & \\ & 1.18666 & \\ & & 0.837813 \end{pmatrix}$	Easy	{0.00722702, -0.0629241, 0.0663058}
			Medium	{0.0924473, -0.0381906, -0.0314611}
			Hard	{0.0522083, 0.0458943, 0.0368333}
2.5	$\begin{pmatrix} 10.0359 & -1.90744 & -12.7735 \\ -1.90744 & 1.40516 & 2.41069 \\ -12.7735 & 2.41069 & 18.7868 \end{pmatrix}$	$\begin{pmatrix} 28.2644 & & \\ & 1.14792 & \\ & & 0.815561 \end{pmatrix}$	Easy	{-0.00708404, 0.0628688, -0.0663512}
			Medium	{-0.0918188, 0.0388391, 0.0318047}
			Hard	{0.053325, 0.0454235, 0.0364544}

2.7	$\begin{pmatrix} 9.30614 & -1.74998 & -11.8202 \\ -1.74998 & 1.33185 & 2.20981 \\ -11.8202 & 2.20981 & 17.426 \end{pmatrix}$	$\begin{pmatrix} 26.183 & & \\ & 1.09764 & \\ & & 0.783334 \end{pmatrix}$	Easy	{0.00697511, -0.0628354, 0.0663787}
			Medium	{0.0925594, -0.0382713, -0.0312228}
			Hard	{0.0520437, 0.0459486, 0.0369047}
3.0	$\begin{pmatrix} 8.38255 & -1.54801 & -10.6134 \\ -1.54801 & 1.24104 & 1.96387 \\ -10.6134 & 1.96387 & 15.7006 \end{pmatrix}$	$\begin{pmatrix} 23.5476 & & \\ & 1.0284 & \\ & & 0.748123 \end{pmatrix}$	Easy	{0.00683515, -0.0627881, 0.0664172}
			Medium	{0.0943257, -0.0367375, -0.0298237}
			Hard	{0.0487892, 0.0472469, 0.037977}
3.2	$\begin{pmatrix} 7.85789 & -1.43679 & -9.93886 \\ -1.43679 & 1.18512 & 1.81667 \\ -9.93886 & 1.81667 & 14.7351 \end{pmatrix}$	$\begin{pmatrix} 22.0696 & & \\ & 0.991988 & \\ & & 0.716497 \end{pmatrix}$	Easy	{0.00670651, -0.0627461, 0.0664512}
			Medium	{0.0949107, -0.036252, -0.0292813}
			Hard	{0.0476594, 0.0476757, 0.0383377}
3.5	$\begin{pmatrix} 7.18392 & -1.29539 & -9.06364 \\ -1.29539 & 1.10822 & 1.63474 \\ -9.06364 & 1.63474 & 13.4846 \end{pmatrix}$	$\begin{pmatrix} 20.1576 & & \\ & 0.93851 & \\ & & 0.680683 \end{pmatrix}$	Easy	{-0.00655523, 0.0626914, -0.0664953}
			Medium	{0.0951373, -0.0361328, -0.029002}
			Hard	{0.0472267, 0.0478378, 0.0384735}
4.0	$\begin{pmatrix} 6.26596 & -1.10699 & -7.88998 \\ -1.10699 & 0.99692 & 1.40403 \\ -7.88998 & 1.40403 & 11.768 \end{pmatrix}$	$\begin{pmatrix} 17.5653 & & \\ & 0.846945 & \\ & & 0.618671 \end{pmatrix}$	Easy	{0.00638886, -0.0626462, 0.0665314}
			Medium	{0.0973162, -0.0338838, -0.0270034}
			Hard	{0.0425815, 0.0495137, 0.0398414}

4.5	$\begin{pmatrix} 5.54616 & -0.973546 & -6.96935 \\ -0.973546 & 0.902769 & 1.23088 \\ -6.96935 & 1.23088 & 10.4105 \end{pmatrix}$	$\begin{pmatrix} 15.5279 & & \\ & 0.771913 & \\ & & 0.559697 \end{pmatrix}$	Easy	{0.00632383, -0.0626331, 0.0665418}
			Medium	{0.0979352, -0.0331905, -0.0263748}
			Hard	{0.0411478, 0.0499974, 0.0402432}
5.0	$\begin{pmatrix} 4.97753 & -0.872742 & -6.24911 \\ -0.872742 & 0.824907 & 1.10127 \\ -6.24911 & 1.10127 & 9.34143 \end{pmatrix}$	$\begin{pmatrix} 13.9288 & & \\ & 0.707142 & \\ & & 0.507891 \end{pmatrix}$	Easy	{-0.00631527, 0.0626283, -0.0665456}
			Medium	{0.0985668, -0.0324114, -0.0257361}
			Hard	{0.0396123, 0.0505119, 0.0406483}
6.0	$\begin{pmatrix} 4.13236 & -0.718729 & -5.16238 \\ -0.718729 & 0.706195 & 0.903467 \\ -5.16238 & 0.903467 & 7.73471 \end{pmatrix}$	$\begin{pmatrix} 11.524 & & \\ & 0.610385 & \\ & & 0.438923 \end{pmatrix}$	Easy	{0.00626113, -0.0626311, 0.0665431}
			Medium	{0.0988602, -0.0320627, -0.0254063}
			Hard	{0.038883, 0.0507305, 0.0408593}
7.5	$\begin{pmatrix} 3.33074 & -0.565914 & -4.06402 \\ -0.565914 & 0.640055 & 0.705241 \\ -4.06402 & 0.705241 & 6.16404 \end{pmatrix}$	$\begin{pmatrix} 9.14703 & & \\ & 0.566733 & \\ & & 0.42107 \end{pmatrix}$	Easy	{0.00621432, -0.0626377, 0.0665377}
			Medium	{0.099047, -0.0318412, -0.0251881}
			Hard	{0.0384123, 0.0508617, 0.041003}
9.0	$\begin{pmatrix} 2.79576 & -0.461742 & -3.3294 \\ -0.461742 & 0.599707 & 0.571542 \\ -3.3294 & 0.571542 & 5.11062 \end{pmatrix}$	$\begin{pmatrix} 7.55536 & & \\ & 0.540344 & \\ & & 0.410381 \end{pmatrix}$	Easy	{0.00614505, -0.0626576, 0.0665214}
			Medium	{0.0998963, -0.030707, -0.0242205}
			Hard	{0.0361582, 0.0515302, 0.0416079}

10.9	$\begin{pmatrix} 2.31839 & -0.3643 & -2.68434 \\ -0.3643 & 0.562566 & 0.455612 \\ -2.68434 & 0.455612 & 4.18864 \end{pmatrix}$	$\begin{pmatrix} 6.15671 & & \\ & 0.512569 & \\ & & 0.400319 \end{pmatrix}$	Easy	{0.00600452, -0.0626223, 0.066549}
			Medium	{0.102128, -0.0272247, -0.0212501}
			Hard	{0.0292955, 0.0534932, 0.0431579}
12.8	$\begin{pmatrix} 1.99887 & -0.302229 & -2.24107 \\ -0.302229 & 0.537728 & 0.375935 \\ -2.24107 & 0.375935 & 3.55747 \end{pmatrix}$	$\begin{pmatrix} 5.2006 & & \\ & 0.496789 & \\ & & 0.396684 \end{pmatrix}$	Easy	{0.00591684, -0.0626317, 0.0665409}
			Medium	{0.102482, -0.0266143, -0.0206744}
			Hard	{0.02805, 0.0537885, 0.0434491}
15.0	$\begin{pmatrix} 1.73316 & -0.250513 & -1.87369 \\ -0.250513 & 0.517752 & 0.314605 \\ -1.87369 & 0.314605 & 3.03663 \end{pmatrix}$	$\begin{pmatrix} 4.41012 & & \\ & 0.482168 & \\ & & 0.395247 \end{pmatrix}$	Easy	{-0.00590602, 0.0626252, -0.066546}
			Medium	{0.103486, -0.0245342, -0.0189807}
			Hard	{0.0240889, 0.054776, 0.0442075}

## 5. Theoretical Calculations

### 5.1. Computational details

All the calculations were based on the structure data of the compound **1-RR**.

All *ab initio* calculations were carried out with MOLCAS 7.8 and are of CASSCF/SO-RASSI/SINGLE\_ANISO type.<sup>S6</sup> Structure of the **1-RR** is shown in Figure S21.

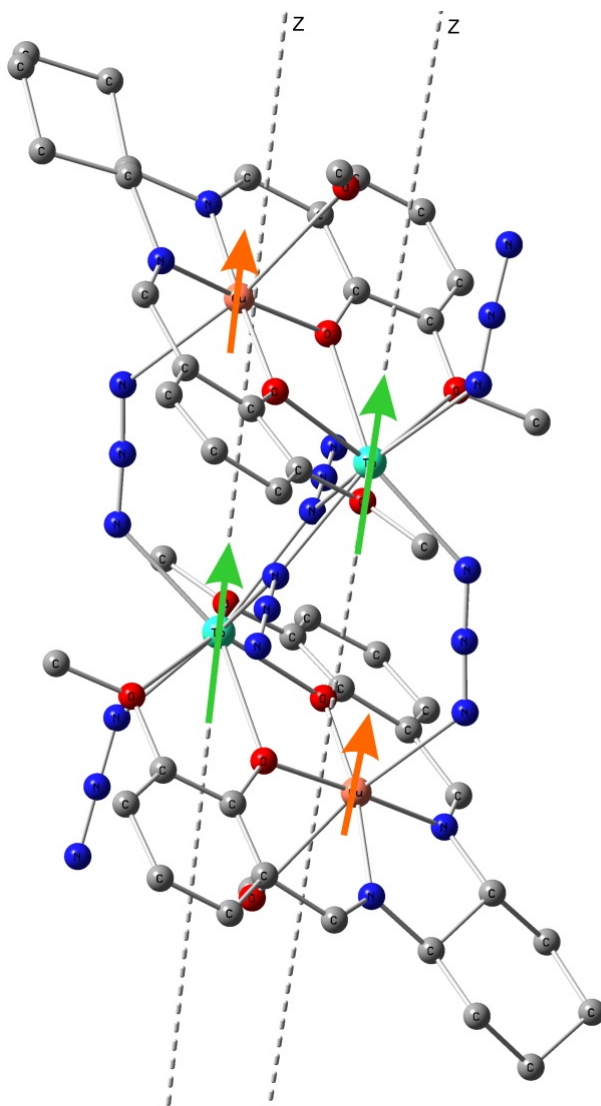


**Figure S21.** Structure of compound **1-RR** for the *ab initio* calculation. The dashed lines correspond to the main magnetic axes of the Tb ions. The arrows show the orientation of local magnetic moments in the ground exchange doublet state.

Each Tb center was calculated using the experimental determined geometry, just substituting the neighboring Tb and Cu ions with diamagnetic analogues, Lu and Zn respectively. Two basis set have been employed. Table S6 shows the contractions of the employed basis sets for all elements.

**Table S6.** Contractions of the employed basis set

<b>Basis 1</b>	<b>Basis 2</b>
Tb.ANO-RCC...7s6p4d2f1g.	Tb.ANO-RCC...8s7p5d3f2g1h.
Lu.ANO-RCC...7s6p4d2f.	Lu.ANO-RCC...7s6p4d2f.
Zn.ANO-RCC...5s4p2d.	Zn.ANO-RCC...5s4p2d.
N.ANO-RCC...3s2p.	N.ANO-RCC...3s2p1d. (close)
O.ANO-RCC...3s2p.	N.ANO-RCC...3s2p. (distant)
C.ANO-RCC...3s2p.	O.ANO-RCC...3s2p1d. (close)
H.ANO-RCC...2s.	O.ANO-RCC...3s2p. (distant)
	C.ANO-RCC...3s2p.
	H.ANO-RCC...2s.

The Cholesky decomposition threshold was set to  $5 \cdot 10^{-8}$ . Active space of the CASSCF method included eight 4f-type electrons spanned by seven 4f orbitals. 7 septet, 140 quintet, 113 triplet and 123 singlet states of Tb ion were mixed by spin-orbit coupling. On the basis of the resulting spin-orbital multiplets, SINGLE\_ANISO program computed local magnetic properties (g-tensors, magnetic axes, local magnetic susceptibility, etc.)

## 5.2. Electronic and magnetic properties of individual Tb center in 1-RR

**Table S7.** Energies ( $\text{cm}^{-1}$ ) of the low-lying spin-orbital states of Tb centers

<b>Spin-orbit energies, <math>\text{cm}^{-1}</math></b>			
<b>Tb1_bas1</b>	<b>Tb1_bas2</b>	<b>Tb2_bas1</b>	<b>Tb2_bas2</b>
0.000	0.000	0.000	0.000
0.003	0.005	0.016	0.013
204.731	223.816	188.860	207.398
206.588	224.351	190.404	207.897
272.983	341.928	257.669	325.037
282.598	350.598	266.846	333.968
347.942	393.305	322.848	369.387
364.101	409.098	340.084	388.349
418.665	457.511	391.613	437.236
425.241	473.864	399.800	443.020
452.598	492.057	426.970	461.610
471.849	512.325	440.797	494.133
476.424	516.868	447.325	494.406

**Table S8.** The  $g_z$  values of the ground and first excited doublets of Tb centers

Multi-plet	Tb1_bas1	Tb1_bas2	Tb2_bas1	Tb2_bas2	
	$g$	$g$	$g$	$g$	
1	$g_z$	17.904318	17.901044	17.882420	17.894037
2	$g_z$	14.664481	14.671135	14.649573	14.641294

### 5.3. Account of magnetic interactions for $\text{Cu}_2\text{Tb}_2$ complex

Copper ions were considered isotropic with a g-factor of 2.1.

The following Hamiltonian has been employed:

$$\hat{H} = -\left(J_{dip}^{Tb1-Tb2} + J_{exch}^{Tb1-Tb2}\right)\tilde{s}_{Tb1,Z}\tilde{s}_{Tb2,Z} - \left(-J_{dip}^{Cu1-Cu2} + J_{exch}^{Cu1-Cu2}\right)\tilde{S}_{Cu1} \cdot \tilde{S}_{Cu2} - 3J_{dip}^{Cu1-Cu2}S_{Cu1,Z}S_{Cu2,Z} - J_{dip}^{Tb1-Cu1}[(1-3\cos^2\theta)\tilde{s}_{Tb1,Z}S_{Cu1,Z} - 3\sin\theta\cos\theta\tilde{s}_{Tb1,Z}S_{Cu1,Y}] - J_{dip}^{Tb2-Cu2}[(1-3\cos^2\theta)\tilde{s}_{Tb2,Z}S_{Cu2,Z} - 3\sin\theta\cos\theta\tilde{s}_{Tb2,Z}S_{Cu2,Y}] - J_{exch}^{Tb1-Cu1}\tilde{s}_{Tb1,Z}S_{Cu1,Z} - J_{exch}^{Tb2-Cu2}\tilde{s}_{Tb2,Z}S_{Cu2,Z} \quad \text{Eq. 1}$$

where  $J_{dip}^{Cu1-Cu2} = \frac{\mu_B^2 g_{Cu}^2}{R_{Cu1-Cu2}^3}$ ;  $J_{dip}^{Tb1-Cu_j} = \frac{\mu_B^2 g_{Tb,Z} g_{Cu}}{R_{Tb1-Cu_j}^3}$ ;  $R$  is the distance between

corresponding metal ions;  $\theta$  is the angle between  $\text{Cu1Tb1}$  direction and the axis  $Z$  (Figure S21).

The magnetic susceptibility was simulated with the program POLY\_ANISO (Figure S4) using the exchange parameters from Table S9 (third column).

**Table S9.** Exchange and dipolar coupling parameters ( $\text{cm}^{-1}$ ) between magnetic ions in **1-RR**. All parameters are reported with respect to the pseudospin  $s = 1/2$  of Tb ions ( $g_{Tb,Z} \sim 18$ ).

	Calculated	Fitted	
	$J_{dip}$	$J_{exch}$ in Eq. (1)	$J$ in Eq. (2)
Tb1-Tb2	2.5	1.8	4.3
Cu1-Cu2	0.003	-3.2	-3.2
Tb1-Cu1	0.4	25.2	25.3
Tb2-Cu2	0.4	25.2	25.3

Due to strong ferromagnetic interactions with the  $\text{Tb}^{\text{III}}$  ions, the copper spins will always be aligned along the  $Z$  axis (Figure S21), parallel to the ground-state magnetic moments of the  $\text{Tb}^{\text{III}}$  ions. Thus, the exchange Hamiltonian [Eq. (1)] acquires a pure Ising form, [Eq. (2)], with parameters given in the last column of Table S9 ( $J$  is calculated from  $J_{exch}$  and  $J_{dip}$ ).

$$\hat{H} = -J_{Tb1-Tb2}\tilde{s}_{Tb1,Z}\tilde{s}_{Tb2,Z} - J_{Tb1-Cu1}\tilde{s}_{Tb1,Z}S_{Cu1,Z} - J_{Tb2-Cu2}\tilde{s}_{Tb2,Z}S_{Cu2,Z} - J_{Cu1,Z-Cu2,Z}S_{Cu1,Z}S_{Cu2,Z} \quad \text{Eq. 2}$$

**Table S10.** Energies (cm<sup>-1</sup>) of the low-lying exchange states of **1-RR**.

<b>Cu<sub>2</sub>Tb<sub>2</sub>_basis_set2</b>		
<b>Energy</b>	<b>Tunneling</b>	<b>g<sub>Z</sub></b>
	<b>Splitting</b>	
0	2.9E-06	39.97
0.405	2.3E-06	1.37
9.239	3.7E-06	35.78
12.437	2.9E-06	35.77
14.523	1.6E-6	4.29
14.540	1.6E-6	4.24
24.861	2.9E-06	31.58
25.474	1.9E-06	1.07
...	...	...
1034.203	0.1	

Ab initio calculated Van-Vleck susceptibility tensor at 3.0 K (in respect to xyz coordinating system as denoted in cif file):

$$\begin{pmatrix} 0.3915 & 0.5470 & -0.7710 \\ 0.5470 & 27.5073 & -38.5324 \\ -0.7710 & -38.5324 & 55.3141 \end{pmatrix}$$

Furthermore, we did Broken Symmetry Density Functional Density (BS-DFT) calculations to estimate the exchange coupling parameters between magnetic centers in compound **1-RR**. We used ORCA 3.0.0 program<sup>S7</sup> in conjunction with B3LYP functional and SVP basis set.<sup>S8</sup> The scalar relativistic effects were taken into account within the second-order Douglas-Kroll-Hess Hamiltonian. We calculated consecutively each of pairs: Cu1-Tb1; Cu1-Tb2; Cu1-Cu2. The terbium ions were substituted by gadolinium ones, which are isotropic, then the obtained exchange coupling parameters calculated for the Cu-Gd pair is rescaled to the spin of Tb ion. When we calculated the Cu1-Cu2 interaction the Tb ions were substituted with Lu ions, which are diamagnetic. When the Cu1-Tb1 pair was considered, the Cu2 and Tb2 were substituted by Zn and Lu, respectively. To note that positions of all atoms were kept as determined experimentally. The Jamaguchi's formula<sup>S9</sup> was employed to calculate the exchange coupling constants:

$$J(i-j) = (E_{HS} - E_{BS}) / (S_{BS}^2 - S_{HS}^2),$$

where HS and BS denote high spin and broken symmetry spin states, respectively.

The following Lines parameters were obtained from BS-DFT calculations:

$$J(\text{Cu1-Tb1}) = +3.68 \text{ cm}^{-1}$$

$$J(\text{Cu1-Tb2}) = +0.22 \text{ cm}^{-1}$$

$$J(\text{Cu1-Cu2}) = -1.85 \text{ cm}^{-1}$$

Considering that the Cu1-Tb2 interaction predicted by BS-DFT is much weaker than the Cu1-Tb1 one, we included in the fitting procedure in POLY\_ANISO just the strongest interaction, in order to avoid the over-parameterization.

## 5.4. Details of electrostatic model calculation.

### 5.4.1. Tb<sup>III</sup> ion electron density

The electron density distribution of the <sup>7</sup>F<sub>6</sub> Ising limit state is described in a linear combination of the axial spherical harmonics Y<sub>2</sub><sup>0</sup>, Y<sub>4</sub><sup>0</sup> and Y<sub>6</sub><sup>0</sup>, with corresponding coefficients as discussed in Siever's publication.<sup>S10</sup> The coefficients of each Y<sub>k</sub><sup>0</sup> are calculated with the following formula, where *J* and *M* denote the total quantum number and magnetic quantum number in the related RS multiplet.

$$c_k = (-1)^{J-M} \frac{7}{\sqrt{4\pi}} \begin{pmatrix} J & k & J \\ -M & 0 & M \\ J & k & J \\ -J & 0 & J \end{pmatrix} \left[ \delta_{k0} + \sqrt{2k+1} \begin{pmatrix} k & 3 & 3 \\ 0 & 0 & 0 \end{pmatrix} \sum_{i=1}^{n-7} (-1)^i \begin{pmatrix} k & 3 & 3 \\ 0 & 4-i & i-4 \end{pmatrix} \right]$$

### 5.4.2. Electrostatic potential

The charges of atoms (Tb, Cu, C, H, O, N) in the molecule was obtained from a DFT calculation, and the positions of the atoms are employed from the single crystal X-ray diffraction data at room temperature without further modification. The electrostatic potential is calculated from the equation described in Huchings' publication (Eq 2.8).<sup>S11</sup>

### 5.4.3. Minimizing the potential energy

By varying the orientation of the quantized axis of one Tb<sup>III</sup> ion in the full Cartesian space, one is able to obtain the electrostatic potential surface with respect to the potential generated by all the atoms in the molecule except for the target Tb<sup>III</sup> ion, as

shown in Figure S24. The global minimum potential energy orientation is considered to be the direction of the magnetization easy axis of one  $\text{Tb}^{\text{III}}$  ion calculated from the electrostatic model. Due to the existence of pseudo inversion center, the environments of the two  $\text{Tb}^{\text{III}}$  ions are nearly identical and the present calculation is not able to provide quantized axis orientation differences.

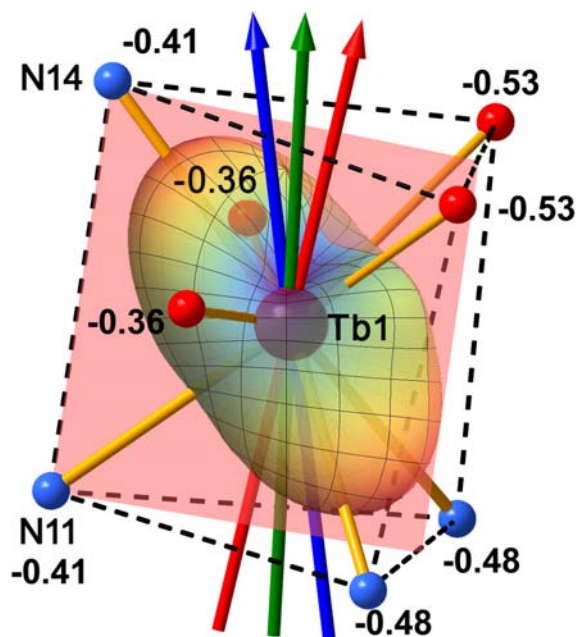


**Figure S22.** The bicapped trigonal prism of the  $\text{Tb}^{3+}$  center and the calculated crystal field potential energy surface. The numbers are the calculated Mulliken charges of the coordination atoms; the blue, green and red arrows represent the easy axes from the experiment, *ab initio* calculation and electrostatic model; and the plane is the pseudo-mirror plane through  $\text{Tb}^{3+}$ .

## 6. References

- (S1) Szlyk, E.; Barwiolek, M.; Kruszynski, R.; Bartczak, T. J. *Inorg. Chim. Acta* **2005**, 358, 3642.
- (S2) Ding, L.; Lin, L. R.; Liu, C. Y.; Li, H. K.; Qin, H. K.; Liu, Y.; Song, L.; Zhang, H.; Tang, B. Z.; Zhao, Y. F. *New J. Chem.* **2011**, 35, 1781.
- (S3) *SAINTE* Version 7.68A, Bruker AXS, Inc.; Madison, WI **2009**.
- (S4) Sheldrick, G. M. *SADABS*, Version 2008/1, Bruker AXS, Inc.; Madison, WI **2008**.
- (S5) Sheldrick, G. M. *SHELXTL*, Version 6.14, Bruker AXS, Inc.; Madison, WI

**2000-2003.**

(S6) (a) Aquilante, F.; DeVico, L.; Ferre, N.; Ghigo, G.; Malmqvist, P. A.; Neogrady, P.; Pedersen, T.B.; Pitonak, M.; Reiher, M.; Roos, B. O.; Serrano-Andres, L.; Urban, M.; Veryazo, V.; Lindh, R. *J. Comput. Chem.* **2010**, *31*, 224; (b) Chibotaru, L. F.; Ungur, L. *J. Chem. Phys.* **2012**, *137*, 064112.

(S7) Neese, F. *The ORCA program system, Wiley Interdiscip. Rev.: Comput. Mol. Sci.*, **2012**, *2*, 73-78.

(S8) (a) Pantazis, D. A.; Chen, X. Y.; Landis, C. R.; Neese, F. *J. Chem. Theory Comput.* **2008**, *4*, 908; (b) Pantazis, D. A.; Neese, F. *J. Chem. Theory Comput.* **2009**, *5*, 2229.

(S9) Yamaguchi, K.; Takahara, Y.; Fueno, T.; in *Smith, V. H. Eds. Applied Quantum Chemistry, V. Reidel, Dordrecht*, **1986**, 155.

(S10) Sievers, J. *Z. Phys. B Con. Mat.* **1982**, *45*, 289.

(S11) Hutchings, M. *Solid State Phys.* **1964**, *16*, 227.